PCCP

Accepted Manuscript

This article can be cited before page numbers have been issued, to do this please use: S. Herrera, A. Y. Tesio, R. Clarenc and E. J. Calvo, *Phys. Chem. Chem. Phys.*, 2013, DOI: 10.1039/C3CP54621G.

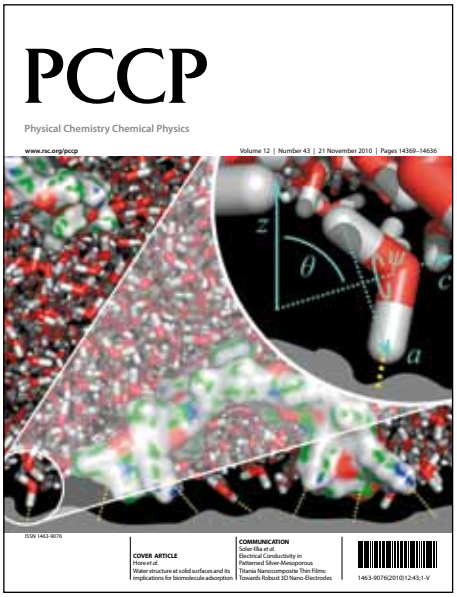

This is an *Accepted Manuscript*, which has been through the RSC Publishing peer review process and has been accepted for publication.

Accepted Manuscripts are published online shortly after acceptance, which is prior to technical editing, formatting and proof reading. This free service from RSC Publishing allows authors to make their results available to the community, in citable form, before publication of the edited article. This *Accepted Manuscript* will be replaced by the edited and formatted *Advance Article* as soon as this is available.

To cite this manuscript please use its permanent Digital Object Identifier (DOI®), which is identical for all formats of publication.

More information about *Accepted Manuscripts* can be found in the **Information for Authors**.

Please note that technical editing may introduce minor changes to the text and/or graphics contained in the manuscript submitted by the author(s) which may alter content, and that the standard **Terms & Conditions** and the **ethical guidelines** that apply to the journal are still applicable. In no event shall the RSC be held responsible for any errors or omissions in these *Accepted Manuscript* manuscripts or any consequences arising from the use of any information contained in them.

Physical Chemistry Chemical Physics

Dynamic Article Links ►
View Article Online
DOI: 10.1039/C3CP54621G

Cite this: DOI: 10.1039/c0xx00000x

www.rsc.org/xxxxxx

ARTICLE TYPE

AFM Study of Oxygen Reduction Products on HOPG in $LiPF_6$ DMSO electrolyte

Santiago E. Herrera,[a] Alvaro Y. Tesio[a] , Romain Clarenc[a] and Ernesto J. Calvo[a]*

Received (in XXX, XXX) Xth XXXXXXXXX 20XX, Accepted Xth XXXXXXXXX 20XX

DOI: 10.1039/b000000x

Ex-situ atomic force microscopy (AFM) has been used to study the morphology of oxygen reduction products from $LiPF_6$ in dimethyl sulfoxide (DMSO) electrolyte, i.e. Li_2O_2 on highly oriented pyrolytic graphite (HOPG) surface. Both cyclic voltammetry and chronoamperometry have shown that at low cathodic polarization the initial deposits decorate the edge steps of HOPG. At higher overpotentials a massive deposit covers the terraces. Upon charging the battery cathode Li_2O_2 oxidation and dissolution does not take place until high overpotentials are reached at which solvent decomposition has been demonstrated by in-situ FTIR studies.

Introduction

The rechargeable Li-air battery exhibits a very large theoretical energy density that can compete with fossil fuels for electric vehicle applications with extended mileage range[1-4]. The non aqueous Li-air battery introduced in 1996 by Abraham[5], consists of a lithium metal anode that dissolves in non aqueous electrolyte and the resulting Li^+ ions react with oxygen reduction products to form insoluble lithium peroxide Li_2O_2 at a porous carbon cathode during discharge. The electrochemical reaction of Li^+ with O_2 to yield insoluble Li_2O_2 in non aqueous electrolyte is reversible sustaining more than ten charge/ discharge cycles.[6]

The electrode kinetics of the oxygen reduction reaction (ORR) in lithium air battery cathodes strongly depends on the solvent[7-9], electrolyte cation[10] and electrode material since the reaction product is solid. On carbon and gold electrodes the first electro-reduction product, superoxide is stable in non aqueous solutions containing tetra alkyl ammonium cations.

Among non aqueous solvents, DMSO with a very large dipole moment and the appropriate geometry to coordinate Li^+ ions has been recently proposed for rechargeable Li-O_2 batteries.[11] Peng et. al. have shown that the Li-air battery can be recharged with 95% capacity retention in 100 cycles using dimethyl sulfoxide (DMSO) electrolyte and porous gold electrode.[12]

On recharging the Li-air battery a large overpotential, ie. > 4 V, is needed to oxidise Li_2O_2 into O_2 and Li^+.[13] At such high potentials DMSO is electrochemically oxidized to dimethyl sulfone on Au above 4.2 V so that it is imperative to reduce the charging overpotential by using a catalyst.

The stability of DMSO with respect to the nucleophillic attack by superoxide ion produced by the oxygen reduction reaction (ORR) in the aprotic solvent has been demonstrated recently by in situ infrared subtractively normalized interfacial Fourier transform infrared spectroscopy (SNIFTIRS) experiments.[14]

Laoire reported the influence of non-aqueous solvents on the electrochemistry of oxygen in rechargeable lithium-air batteries[7] and compared the ORR in acetonitrile and DMSO electrolytes containing lithium ions. Trahan et. al.[9] reported studies of Li-Air cells in dimethyl sulfoxide-based electrolyte using the rotating disc (RDE) and rotating ring disc electrode (RRDE) and demonstrated that unlike acetonitrile in DMSO electrolyte soluble superoxide radical anion, O_2^-, can be collected at the ring electrode of the RRDE.

In a recent communication we reported that soluble superoxide radical anion can be detected at a ring electrode of a RRDE system in lithium solutions of acetonitrile containing 0.1 M DMSO, unlike in pure acetonitrile electrolytes which show no evidence of producing soluble O_2^-.[15] Therefore the stronger solvation of Li^+ in DMSO with respect to CH_3CN stabilizes solvated Li-O_2^- ion pairs.

Highly oriented pyrolytic graphite (HOPG) is a model system for carbon electrode material with low reactivity in the basal plane terraces and reactive groups at the step edges.[16] Composites based on graphene have been recently reported for Li-O_2 battery cathodes.[17-19] In situ AFM study of Li-O_2 cathode reduction products on highly oriented pyrolytic graphite (HOPG) has been reported recently.[20] In the present communication we present preliminary ex-situ AFM studies of the oxygen reduction insoluble products deposited on HOPG electrode surfaces in O_2 saturated $LiPF_6$ DMSO electrolyte.

Experimental

Anhydrous dimethyl sulfoxide (DMSO) ≥ 99.9% (SIGMA-ALDRICH), lithium hexafluorophosphate battery grade, ≥99.99% trace metals basis (ALDRICH), were stored in the argon-filled MBRAUN glove box with the oxygen content ≤0.1 ppm and water content below 2 ppm. DMSO was dried for several days

View Article Online
DOI: 10.1039/C3CP54621G

over 3 Å molecular sieves, (SIGMA-ALDRICH); all solutions were prepared inside of the glove box and the water content was measured using the Karl Fisher 831 KF Coulometer (Metrohm). Solutions were found to contain initially around 50 ppm of water.

A three electrode EC-AFM electrochemical cell was built using Teflon^R and a Kalrez o-ring pressed onto HOPG sample with a 0.64 cm^2 area. The auxiliary electrode was a Pt gauze (Goodfellow PT008710/43) and the reference electrode was a Pt wire coated with a $LiMn_2O_4/Li_2Mn_2O_4$ in the same Li^+ electrolyte.[21] The reference electrode potential measured in a glove box with respect to a lithium foil in the solution was 3.25 V and all potentials herein are referred to this electrode. The cell was contained in a glass cylinder environmental chamber filled with dry oxygen.

Electrochemical cyclic voltammetry and chronoaperometry experiments were carried out with a potentiostat/ galvanostat coupled with the AFM (EC-AFM, Agilent 5500 AFM /SPM).

The HOPG surface was scanned by AFM using and insulating triangular Si tip PointProbe® Plus Non-Contact / Soft Tapping Mode (radius < 10 nm force constant 48 N.m^{-1}, resonance frequency 157.85 kHz) using non contact mode. In a typical experiment after the electrochemical treatment the HOPG surface was rinsed with 10 100 µL DMSO aliquots and dried under Ar. Image analysis was performed with Gwyddion 2.33 software (http://hwyddion.net/). Prior to each new experiment the HOPG was defoliated by using the scotch tape usual procedure.

Results and Discussion

Figure 1A depicts the cyclic voltammetry for the reduction of molecular oxygen in 0.1 M $LiPF_6$ in DMSO at 0.1 V.s^{-1} on an HOPG surface. The starting and end potentials are shown in the Figure. A reduction peak at c.a. 2.3 V is apparent with no passivation of the surface in the back potential sweep. This contrasts with the case of GC or Au where no current is seen on the reverse sweep.[9, 22] Integration of the cathodic current peak yields 1.1 mC.cm^{-2}. Notice in the reverse sweep an anodic peak at c.a. 2.6 V which is due to the oxidation of superoxide radical ion on the surface.[7, 22] Peng et. al.[12] have shown by infrared and Raman spectroscopies that lithium peroxide is formed during the O_2 reduction on nanoporous gold electrodes in DMSO electrolyte.

Unlike in several electrolytes including acetonitrile, in DMSO superoxide ion is stabilized in the presence of lithium ions due to the preferential solvation of the small cation by this solvent.

Further excursion in the positive potential shows another anodic process of re-oxidation of the surface O_2 reduction products and anodic oxidation of the solvent.[14] It is worth mentioning that the deposit depicted in Figure 1B was obtained after the HOPG electrode was scanned at positive potentials (see start and end points) and still nanoparticles were observed on the surface. If the positive potential scan is restricted to 3,5 V thus not allowing the electrode to reach the anodic region, the same nanoparticle pattern is observed. This suggests that the anodic oxidation of Li_2O_2 on HOPG surfaces is not very efficient.

The AFM blank HOPG image at potentials positive to the onset of ORR is characterized by atomically flat terraces and step edges.

An ex-situ AFM image of HOPG surface after the cathodic peak is depicted in Figure 1B and it is clear that the step edges are

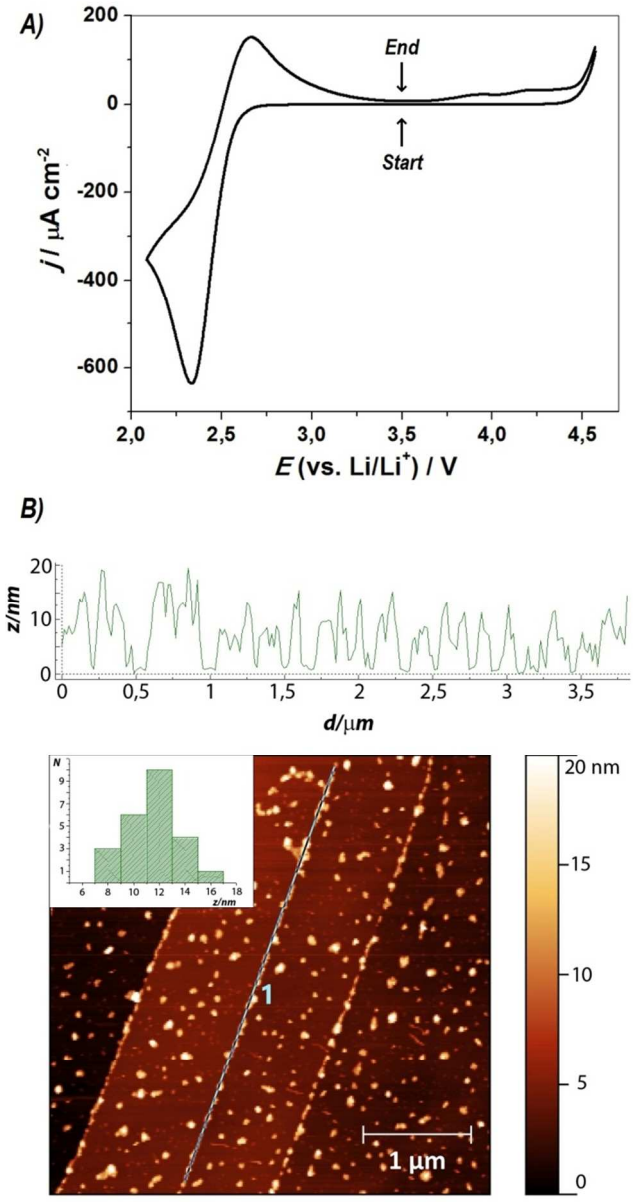

Figure 1. A. Cyclic voltammetry of HOPG in 0.1 M $LiPF_6$ in DMSO at 0.1 V.s^{-1}. B: AFM image of HOPG surface after the cathodic O_2 reduction peak.

decorated by nanoparticles, most likely Li_2O_2, but also the nanoparticles are seen on the basal plane steps. The profile and statistics insets show that the deposit particles are less than 12 nm in height. Notice that an important fraction of the HOPG surface is not covered under these conditions.

Potential step transients from the open circuit potential to 2.65 and 2.05 V are depicted in Figures 2 and 3 respectively with their corresponding AFM images and selected height profiles.

At 2.65 V in the ORR onset small reduction currents and a small charge density of 0.54 mC.cm^{-2} in 150 seconds can be seen while at 2.05 V after the cathodic peak in Figure 1 we recorded 15

View Article Online
DOI: 10.1039/C3CP54621G

mC.cm^{-2}. Notice in both cases that after 150 seconds the oxygen reduction current does not drop to zero, consistent with the Li_2O_2 precipitation of Li_2O_2 to occur. On the other hand, $Li^+O_2^-$ ion pairs on the surface readily disproportionate due to the electron catalysis by the conducting surface, i.e. the exchange of electrons

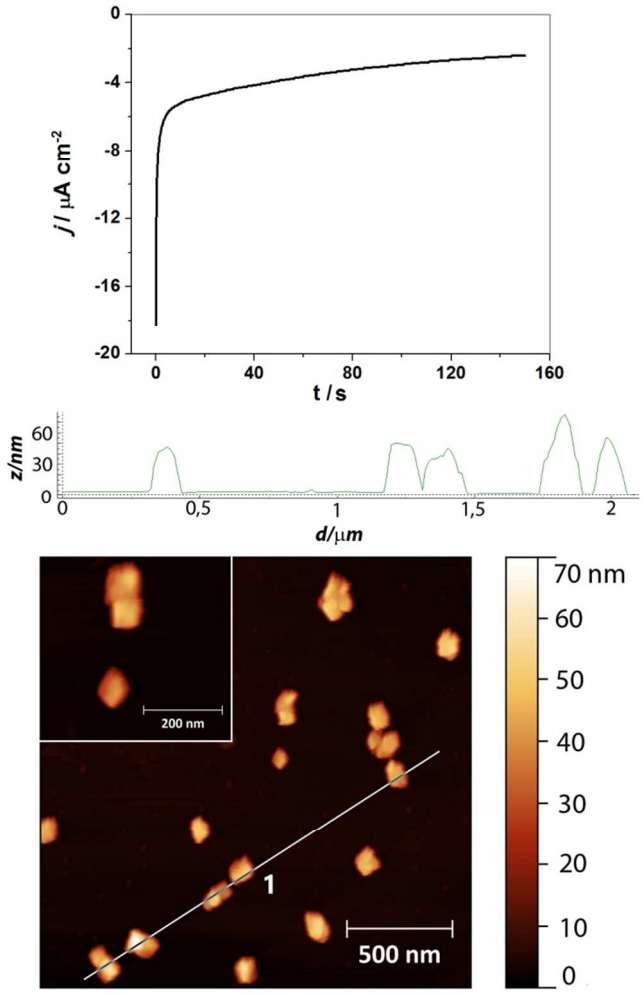

Figure 2. A. Chronoamperometry of HOPG in O_2 saturated $LiPF_6$ in DMSO at 2.65 V. B. AFM image of HOPG surface after 150 s polarization at 2.65 V. Line profile of deposit.

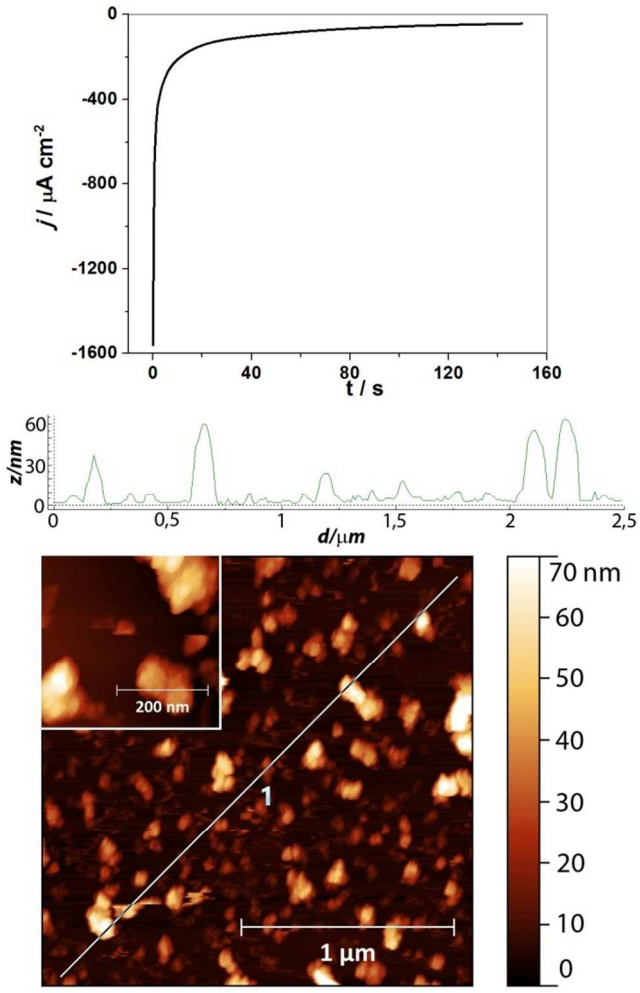

Figure 3. A. Chronoamperometry of HOPG in O_2 saturated $LiPF_6$ in DMSO at 2.65 V. B. AFM image of HOPG surface after 150 s polarization at 2.65 V. Line profile of deposit.

low coverage, i.e. there is no passivation of the cathode by the insoluble O_2 reduction product. However, at 2.05 V the surface is completely covered by crystals of the O_2 reduction products.

The first step of the O_2 reduction in aprotic solvents is the formation of the radical anion superoxide O_2^-.[23] In electrolytes with low polarizing cations, i.e. tetralkyl ammonium salts the reaction is outer sphere.[24] However in Li^+ containing electrolytes in many solvents contact ion pairs, $O_2^-{}_{solv}Li^+{}_{solv}$, are formed and under the strong polarization of O_2^- by Li^+ disproportionation to lithium peroxide and oxygen takes place.

$$O_2 + Li^+ + e^- \rightarrow [O_2^-]_{DMSO}[Li^+]_{DMSO} \qquad (1)$$

DMSO preferentially solvates Li^+ ions leading to a non contact ion pair. In solvents weakly solvating the cation, contact ion pair at shorter distance, leads to electron reorganization in a dimer transition state and Li_2O_2 and O_2 result from disproportionation.

If this happens in the solution adjacent to the electrode we expect at the HOPG surface. Note that both O_2^- and Li^+ ion pairs need not be adjacent since the electrons can be easily shuttled on the conductive surface from one ion pair to another. Nucleation of nanoparticles at step edges is apparent from Figures 1-3 where abundant active sites are available. Unlike bimolecular disproportionation of soluble species the conductive electrode surface catalyzes the reaction.

Some recent DFT calculations of Li_2O_2 adsorption on graphene surfaces have shown that the lithium peroxide monomer is weakly adsorbed on the graphene substrate, i.e. a low binding energy of -0.26 eV but it binds strongly at defects, in particular those bearing carboxylate groups.[17] Further aggregation of Li_2O_2 monomers occurs at the surface:

$$(Li_2O_2)_{n-1} + Li_2O_2 \rightarrow (Li_2O_2)_n \qquad (2)$$

View Article Online
DOI: 10.1039/C3CP54621G

The weakly adsorbed lithium peroxide would be mobile on the HOPG surface and easily migrate and aggregate until it reaches a defect or step edge.

is the efficient oxidation of the solid Li_2O_2 accumulated during discharge in the porous carbon structure.[26]

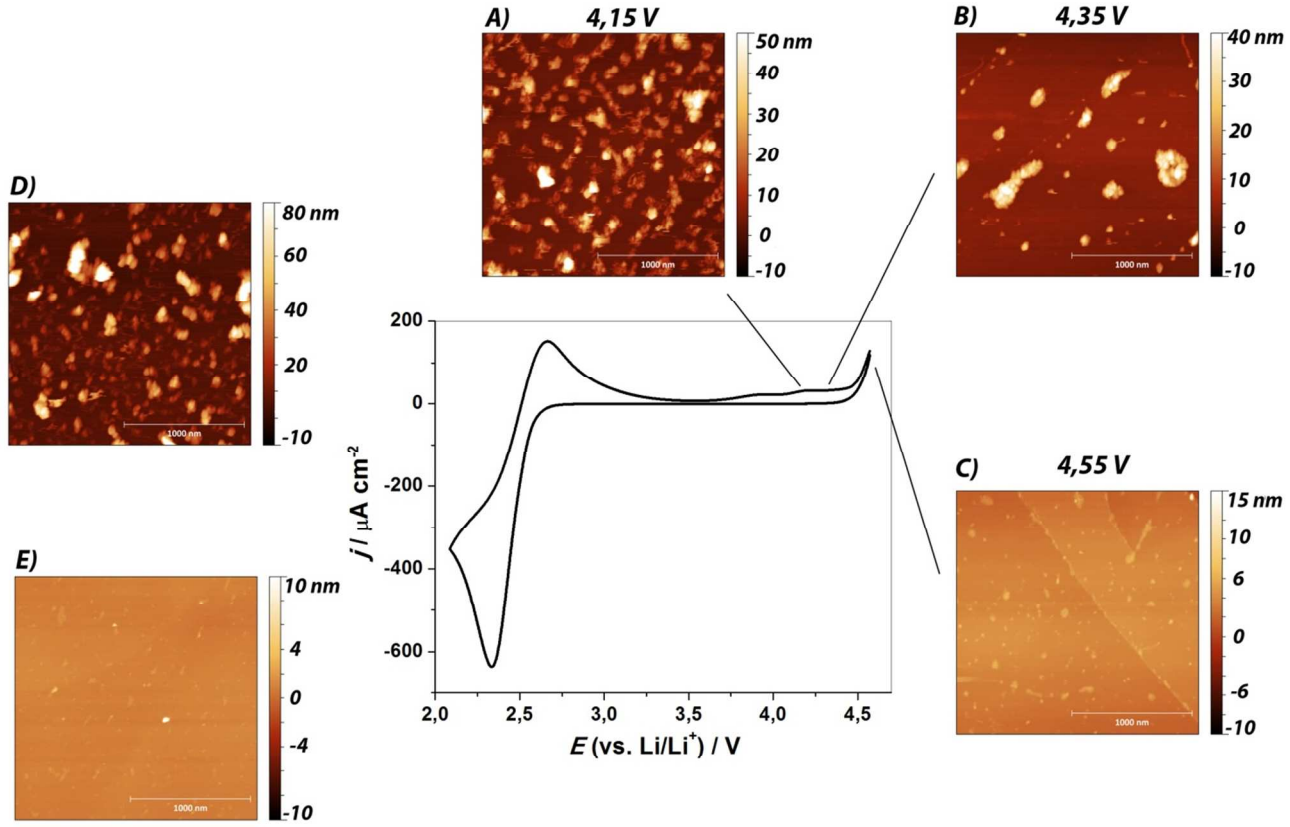

Figure 4. Cyclic voltammetry of HOPG in O_2 saturted 0.1 M $LiPF_6$ at 0.1 $V.s^{-1}$ Pannels A, B and C depict the surface morphology at different applied potential steps from 2.05V (see Figure 4D) to the final potentials indicated above each panel during 150 second step in the cathodic oxygen reduction region. Panel E corresponds to the blank at 3.5 V before the cathodic scan (start).

At low overpotentials, in the onset of the ORR wave, i.e. 2.65 V most likely the reactions at the HOPG surface are:

$$O_2 + Li^+ + e^- \rightarrow \quad [O_2^- Li^+] \quad (3)$$

$$2[\,O_2^- Li^+] \rightarrow Li_2O_2 + O_2 \qquad (4)$$

with very little deposit as seen in Figure 2. At high overpotential, however, i.e. 2.6 V a sequential two one-electron transfer steps is most likely, ie. eqn. 3 followed by:

$$O_2^+ Li^+ + Li^+ + e^- \rightarrow Li_2O_2 \quad (5)$$

And yields massive deposition of Li_2O_2 as seen in Figure 3.

In the present study with DMSO lithium ion containing electrolyte we have not detected nanoplates but individual aggregated geometric nanocrystals. Notice that spherical shape nanoparticles characteristic of diffusion controlled aggregation have not been observed.

In cyclic voltammetry the height of the O_2 reduction products nanocrystals never exceeds 12 nm in good agreement with previous reports[20] and predicted values by theory taking into account the limited charge transport in Li_2O_2 with low electronic conductivity via electron tunneling.[25]

One of the major challenges for the success of the Li-O_2 battery

The potential gap of more than one volt between discharge and charge curves in a Li-O_2 battery arises from the slow kinetics and large overpotential for the re-oxidation of Li_2O_2. Several catalysts have been suggested to solve this problem.[27] Shao-Horn and co-workers, have recently reported the influence of the morphology and structure of Li_2O_2 deposits in discharged battery cathodes on the O_2 evolution kinetics during re-charge.[13]

Figure 4 shows during the positive direction potential scan an anodic peak at 2.6 V due to the oxidation of soluble solvated O_2^- adjacent to the electrode which is characteristic of DMSO electrolytes.[9] With the rotating ring disc electrode under convective-diffusion conditions this peak is not observed since the radical anion is swept away from the electrode, nor it is detected at the ring electrode downstream.[28]After this peak there is no significant anodic current until very positive potentials and then solvent decomposition by electrochemical oxidation to dimethyl sulfone is apparent above 4.3 V.[14]

The different panels in Figure 4 show the evolution of the surface morphology after potentiostatic treatment during 150 seconds of the surface that results from the oxygen reduction at 2.05 V for 150 seconds: 4.15, 4.35 and 4.55 V. At 2.05 V a dense Li_2O_2 deposit formed by nanocrystals with an average height of 60 nm covers the HOPG surface. Polarization at 4.15 V for 150 seconds results in the dissolution of the largest nanoparticles but a

View Article Online
DOI: 10.1039/C3CP54621G

significant deposit remains on the surface as can be seen from the different z-scales in panels A and D.

At 4.35 V most of the nanoparticles have been re-oxidized and the remaining lie on step edges. Notice also some aggregation leading to larger structures. Finally at 4.55 V most of the lithium peroxide deposit has been eliminated but at such positive potentials substantial simultaneous oxidation of the DMSO takes place.[14]

Conclusions

We have investigated the morphology of oxygen reduction insoluble products in DMSO $LiPF_6$ electrolyte by ex-situ AFM on HOPG after treatment at different electrode potentials for the oxygen reduction (discharge) and oxygen evolution by Li_2O_2 oxidation (charge). Decoration of step edges is apparent and also deposits at basal plane terraces grow by peroxide aggregation. At low cathodic polarization few crystals are observed probably by disproportionation of superoxide, while a massive deposit is observed at high polarization due to two one-electron transfer to the oxygen molecule. Re-oxidation of Li_2O_2 and thus recovery of the HOPG surface does not take place until very positive potentials are reached. However, at these potentials DMSO is electrochemically oxidized to dimethyl sulfone. Therefore, efficient catalysts are required for the charging reaction.

Acknowledgements

S.H, R.C and A.Y.T. acknowledge research doctoral and post-doctoral grants from CONICET, E.J.C. is a permanent research Fellow of CONICET, Argentina. Research grants from Fonarsec FS-Nano 07 and PICT 2008-2937 are gratefully acknowledged.

Notes and references

[a] *INQUIMAE, Facultad de Ciencias Exactas y Naturales, Universidad de Buenos Aires, Pabell'on 2, Ciudad Universitaria, AR-1428 Buenos Aires, Argentina. Fax: 541145763304; Tel: 541145763380; E-mail: calvo@qi.fcen.uba.ar*

[b] *Address, Address, Town, Country. Fax: XX XXXX XXXX; Tel: XX XXXX XXXX; E-mail: xxxx@aaa.bbb.ccc*

† Electronic Supplementary Information (ESI) available: Details of the EC-AFM cell and AFM images of blank surfaces are include in the SI: See DOI: 10.1039/b000000x/

References

1. P. G. Bruce, S. A. Freunberger, L. J. Hardwick and J.-M. Tarascon, *Nature Materials*, 2012, **11**, 19.
2. J. Christensen, P. Albertus, R. S. Sanchez-Carrera, T. Lohmann, B. Kozinsky, R. Liedtke, J. Ahmed and A. Kojic, *Journal of the Electrochemical Society*, 2012, **159**, R1-R30.
3. L. J. Hardwick and P. G. Bruce, *Current Opinion in Solid State & Materials Science*, 2012, **16**, 178-185.
4. K. M. Abraham, in *Lithium Batteries: Advanced Technologies and Applications*, ed. K. M. A. Bruno Scrosati, Walter van Schalkwijk, and Jusef Hassoun, John Wiley & Sons, Inc, First edn., 2013.
5. K. M. Abraham and Z. Jiang, *Journal of the Electrochemical Society*, 1996, **143**, 1-5.
6. T. Ogasawara, A. Debart, M. Holzapfel, P. Novak and P. G. Bruce, *Journal of the American Chemical Society*, 2006, **128**, 1390-1393.
7. C. O. Laoire, S. Mukerjee, K. M. Abraham, E. J. Plichta and M. A. Hendrickson, *Journal of Physical Chemistry C*, 2010, **114**, 9178-9186.
8. B. D. McCloskey, D. S. Bethune, R. M. Shelby, G. Girishkumar and A. C. Luntz, *Journal of Physical Chemistry Letters*, 2011, **2**, 1161-1166.
9. M. J. Trahan, S. Mukerjee, E. J. Plichta, M. A. Hendrickson and K. M. Abraham, *Journal of the Electrochemical Society*, 2013, **160**, A259-A267.
10. C. O. Laoire, S. Mukerjee, K. M. Abraham, E. J. Plichta and M. A. Hendrickson, *Journal of Physical Chemistry C*, 2009, **113**, 20127-20134.
11. D. Xu, Z.-l. Wang, J.-j. Xu, L.-l. Zhang and X.-b. Zhang, *Chemical Communications*, 2012, **48**, 6948-6950.
12. Z. Peng, S. A. Freunberger, Y. Chen and P. G. Bruce, *Science*, 2012, **337**, 563-566.
13. B. M. Gallant, D. G. Kwabi, R. R. Mitchell, J. Zhou, C. V. Thompson and Y. Shao-Horn, *Energy & Environmental Science*, 2013, **6**, 2518-2528.
14. Mozhuzhukina N, Mendez De Leo L.P. and E. J. Calvo, *Journal of Physical Chemistry C, doi 10.1021*, 2013, **in press**.
15. E. J. Calvo and N. Mozhzhukhina, *Electrochemistry Communications*, 2013, **31**, 56-58.
16. R. J. Bowling, R. T. Packard and R. L. McCreery, *Journal of the American Chemical Society*, 1989, **111**, 1217-1223.
17. J. Xiao, D. Mei, X. Li, W. Xu, D. Wang, G. L. Graff, W. D. Bennett, Z. Nie, L. V. Saraf, I. A. Aksay, J. Liu and J. G. Zhang, *Nano Letters*, 2011, **11**, 5071-5078.
18. E. Yoo and H. Zhou, *ACS Nano*, 2011, **5**, 3020-3026.
19. Y. Li, J. Wang, X. Li, D. Geng, R. Li and X. Sun, *Chemical Communications*, 2011, **47**, 9438-9440.
20. R. Wen, M. Hong and H. R. Byon, *Journal of the American Chemical Society*, 2013, **135**, 10870-10876.
21. J. M. Tarascon and D. Guyomard, *Journal of the Electrochemical Society*, 1991, **138**, 2864-2868.
22. C. O. Laoire, S. Mukerjee, E. J. Plichta, M. A. Hendrickson and K. M. Abraham, *Journal of the Electrochemical Society*, 2011, **158**, A302-A308.
23. A. S. D.T. Sawyer, J.L. Roberts ,Jr., *Electrochemistry for Chemists*, John Wiley & Sons Inc., New York, 1995.
24. M. S. Hossain, D. Tryk and E. Yeager, *Electrochimica Acta*, 1989, **34**, 1733-1737.
25. V. Viswanathan, K. S. Thygesen, J. S. Hummelshoj, J. K. Norskov, G. Girishkumar, B. D. McCloskey and A. C. Luntz, *Journal of Chemical Physics*, 2011, **135**.
26. Y. Chen, S. A. Freunberger, Z. Peng, O. Fontaine and P. G. Bruce, *Nature Chemistry*, 2013, **5**, 489-494.
27. A. Débart, A. J. Paterson, J. Bao and P. G. Bruce, *Angewandte Chemie - International Edition*, 2008, **47**, 4521-4524.
28. W. Torres, N. Mozhzhukhina, A. Y. Tesio and E. J. Calvo, *J. Physical Chemistry C*, 2013, **submitted**.

View Article Online
DOI: 10.1039/C3CP54621G

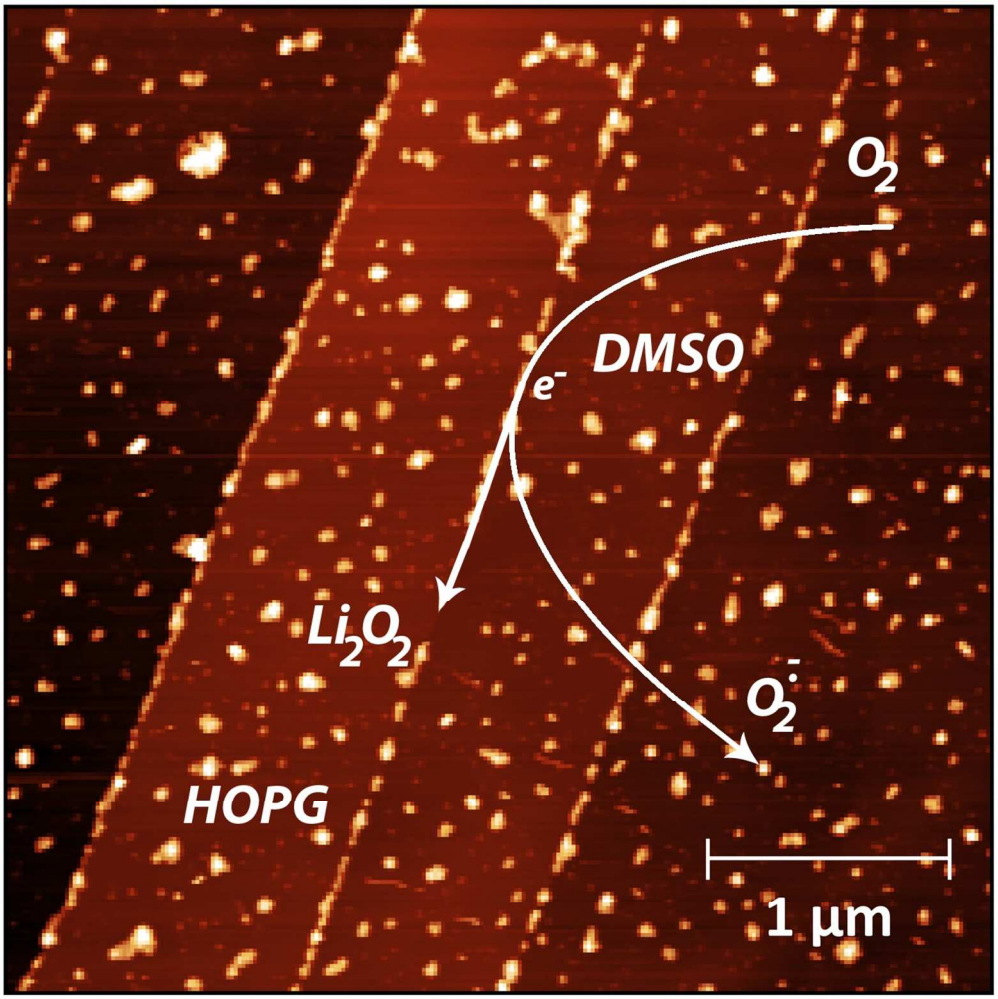

377x376mm (96 x 96 DPI)